Universitat Politècnica de Catalunya (UPC)
Universitat Autònoma de Barcelona (UAB)
Universitat de Barcelona (UB)
Institut de Ciències Fotòniques (ICFO)

http://www.photonicsbcn.eu

Master in Photonics

MASTER THESIS WORK

QUANTUM FREQUENCY CONVERSION OF SINGLE PHOTONS FROM 606NM TO TELECOM WAVELENGTHS FOR HETEROGENEOUS QUANTUM NETWORKS

Josep Maria Batllori Berenguer

Supervised by Prof. Hugues de Riedmatten, (ICFO)

Presented on date 19th November 2020

Registered at

Escola Tècnica Superior d'Enginyeria de Telecomunicació de Barcelona

Quantum frequency conversion of single photons from 606nm to telecom wavelengths for heterogeneous quantum networks

Josep Maria Batllori Berenguer

ICFO - Institut de Ciències Fotòniques, The Barcelona Institute of Science and Technology, 08860 Castelldefels (Barcelona), Spain

E-mail: Josep-Maria.Batllori@icfo.eu

November 19, 2020

Abstract. In this work we experimentally and theoretically characterize the converted signal and the noise level of a quantum frequency conversion (QFC) device implemented for frequency down conversion from the visible to telecommunication wavelengths. This frequency converter is a useful device able to interface quantum memories operating at different wavelengths. We observe that the main noise source is directly induced by the pump via spontaneous parametric down-conversion (SPDC), enhanced by imperfections in the periodic poling structure of the waveguide. We also measure conversion with high signal to noise ratio for microsecond long weak coherent states at the single photon level. Finally, we show theoretically that the converted Stokes/Anti-Stokes non-classical correlations of photon pairs emitted by quantum memories could be largely preserved for pulse durations lower than 4μs.

Keywords: quantum frequency conversion, quantum memories, single photons.

1. Introduction

Quantum information science (QIS) is an emerging research field that explores new ways of computing and processing information that can be encoded in quantum systems. QIS relies on quantum physics effects to encode and transmit information. In quantum communication, information is encoded in the form of quantum bits and transmitted through quantum networks. In the long-distance range two types of networks are generally implemented: one entirely based on optical fibers and the other using free-space transmission. In fiber transmission, signal losses represent a big issue over long distances. Unlike classical networks, the signal cannot be amplified due to the no-cloning theorem [1], which states that it is impossible to copy quantum information without degrading the fidelity.Moreover, other issues arise such as the presence of noise, quantum decoherence effects sensitive to environmental events and quantum correlations limited by dispersion and absorption effects.

A proposal for the distribution of quantum states over long distances is the use of quantum repeaters [2], which rely on the division of the total distance into several segments called elementary links. Entanglement is first distributed within the elementary links, stored in quantum memories, and then extended towards larger distances by entanglement swapping. Once the entanglement has been expanded over long distances, it can be used to transmit a qubit by quantum teleportation [3], or to perform entanglement-based quantum key distribution. To create entanglement within an elementary link, a crucial resource is to have entanglement between a quantum memory and a photon at telecommunication wavelengths, where fiber losses are the lowest. several protocols for quantum repeaters exist, being one of the most relevant the Duan-Lukin-Cirac-Zoller (DLCZ) protocol [4].

Several different types of quantum network nodes have been proposed, which have different capabilities, e.g. single trapped ions, cold atoms, rare-earth doped solids, NV-centers in diamond, etc. For example, solid-state quantum memories based on rare-earth doped solids are good quantum memories with large multiplexing capability [5], and single trapped ions are excellent for quantum processing [6], but can currently only interact efficiently with ultranarrowband photons (of order of 100 kHz bandwidth). The long term goal of the current project is to develop a quantum interface allowing to combine these two kinds of quantum nodes which operate at very different wavelengths and bandwidth. Towards this goal, the main objective of this Master thesis is to demonstrate a quantum frequency conversion interface at the single photon level from the visible to telecommunication wavelength, for microsecond long pulses. We also aimed at showing theoretically that the device could be used with quantum light emitted by a solid-state quantum memory.

The report is organized as follows. In section (2) we settle the starting point, explaining the quantum frequency conversion process. In section (3) we introduce the quantum memory protocol of interest, called DLCZ-AFC. Section (4) describes the optical setup used for down-converting the signal to telecom wavelengths. In section (5), we characterize our QFC device in terms of noise and SNR employing weak coherent states (WCS). Finally, in section (6) we analyze theoretically the non-classical correlations via the DLCZ-AFC protocol.

2. Quantum frequency conversion (QFC)

The use of quantum memories for entanglement distribution and swapping requires the connection to optical fibers and most of them operate the visible ornear-IR wavelength range. QFC allows to translate the wavelength of the quantum states of light while preserving their quantum properties (e.g. phase coherence and photon statistics). Thus, heterogeneous quantum networks operating at different wavelengths can be created. QFC techniques [7] applied for converting light to the telecom band are practical tools for interfacing distant memories, which operate at different wavelengths, using the telecom wavelength as an intermediary, due to low loss in optical fibers (0.2 dB/Km). Although

QFC can be performed for both up-conversion or down-conversion of quantum states, in this thesis we implement QFC to convert light from the visible to the telecom region at the single-photon level. In this work, we use weak coherent states to mimic single photons and then characterize the frequency conversion process in the quantum regime.

In our group, we use Pr^{+3}:Y_2SiO_5 crystals at 606 nm wavelength. The approach chosen in this thesis is based on frequency conversion via difference frequency generation (DFG) in a material with $\chi^{(2)}$ non-linearity. We use a periodically poled lithium niobate (PPLN) waveguide [8], based on the quasi-phase-matching (QPM) technique.

In DFG an input quantum state at wavelength λ_s=606 nm is coupled with a strong pump field at λ_p=994 nm inside a non-linear crystal. This signal is down-converted to the telecom spectrum region (λ_T=1552 nm) via a three-wave mixing process. The down-conversion of the signal light is restricted by the energy conservation of the process ($\frac{1}{1552} = \frac{1}{606} - \frac{1}{994}$). That conversion has been already demonstrated [7], but for short photons (200 ns). The objective of this QFC experiment is to simultaneously achieve high conversion efficiency and high signal-to-noise ratio (SNR) at the telecom spectral region for converting long photons (> 1 μs) generated by a quantum memory [9].

3. Quantum memories based on DLCZ-AFC protocol

In this project we seek to implement an emissive quantum memory protocol called AFC-DLCZ, which combines the DLCZ and Atomic frequency comb (AFC) schemes, in solid-state quantum memories (QMs). The DLCZ quantum protocol is based on a three-level atomic configuration with one excited state and two metastable ground states [4]. The aim is to produce a single collective spin excitation addressing off-resonantly the excited state $|e\rangle$, via spontaneous Raman scattering by sending a weak write pulse. The later detection of a photon, called Stokes photon, heralds the storage of that excitation in the form of a spin-wave in the ground state level $|s\rangle$. A strong read pulse, resonant with the $|s\rangle - |e\rangle$, can be sent in order to transfer efficiently the spin-wave to the original ground state $|g\rangle$, by emitting a single photon, called Anti-Stokes photon. The AFC is a quantum protocol that can be applied as an absorptive memory, generally in a two-level atomic system [10]. It is based on tailoring the inhomogeneous broadened line of the optical transition $|g\rangle - |e\rangle$ using a frequency comb pattern, with frequency periodicity Δ and highly absorptive peaks. When an incoming photon of linewidth $\gamma >> \Delta$ is sent, it is absorbed by the peaked structure and retrieved as an echo after a time $\tau = 1/\Delta$.

There is a lot of interest in the application of DLCZ protocol in rare-earth doped crystals since they provide exceptional optical and coherence properties [11]. The main issue is the impossibility to shine an off-resonant pulse on the transition $|g\rangle - |e\rangle$ due to the weak dipole moment in solid-state environments. One potential strategy is the implementation of the AFC-DLCZ protocol [9]. The storage of the optical excitation relies on a AFC in the broadened transition to avoid the loss of coherence of the excited ions. The procedure is analogous to the standard DLCZ protocol except from the fact that we now send a weak pulse on-resonant with the transition $|g\rangle - |e\rangle$. A Stokes photon,

resonant to the $|e\rangle - |s\rangle$, is then generated by spontaneous emission and is correlated with the creation of a spin-wave in the crystal. By sending a strong read pulse, the rephasing of the Stokes photon is resumed inside the AFC, emitting its echo called anti-Stokes photon. In fact, the Anti-Stokes photon emission time is non-classically correlated with the emission time of the previously emitted Stokes photon. The phase-matching condition holds $k_W + k_R - k_S - k_{AS} = 0$, where k_W, k_R, k_S, k_{AS} are respectively the wavevectors of the write pulse, the read pulse, the Stokes and Anti-Stokes photons.

4. Optical setup

The down-conversion configuration used for QFC is represented in Figure (1). The 606 nm signal light is sent within single mode fibers (SMF). A double-pass acousto-optical modulator (AOM) is used to gate and tune the signal power. The polarization is later adjusted with a polarization controller (PC). After the fiber coupler, a polarizing beam splitter (PBS) followed by a half-waveplate ($\lambda/2$) are placed to ensure that there is no change in polarization. The signal is then reflected by a dichroic mirror (DM), which simultaneously transmits the pump field, and enables to overlap both modes before coupling into the waveguide. The 994 nm light comes from a laser diode. The amplified light is then sent through a polarization-maintaining (PM) optical fiber that cleans the spatial mode. The power and polarization of the pump beam is controlled by placing a $\lambda/2$ waveplate followed by a PBS and again another half-waveplate.

For this project we use a ridge-waveguide in a Lithium Niobate (LN) crystal. The waveguide is stabilized at a temperature of 66 degrees Celsius and has a length of 1.4 cm. Two aspheric lenses situated at the input and output of the waveguide enable to couple and out-couple respectively, with two XYZ translation stages, the incoming light. The converted telecom mode is then selected by filtering out the non-converted 606 nm and 994 nm light by using two dichroic mirrors, which also transmit telecom light. The telecom light is spectrally filtered employing an etalon filter (95% transmission, 210 MHz bandwidth, 4 GHz free-spectral range (FSR)) and a fiber Bragg Grating (FBG) (65% transmission, 2.5 GHz bandwidth). We have also installed a telecom band-pass filter (92%transmission) in order to increase our extinction ratio for the noise when measuring the signal. Finally, we use a single photon detector (SPD) (InGaAs APD, 10% efficiency, 10 Hz dark counts) to measure the converted noise or signal counts of our converter.

5. QFC characterization with weak coherent states

In this section we want to estimate the performance of our QFC device. To this aim, we characterize the converter with weak coherent states of light (WCS), by attenuating the laser light until reaching an approximated value of 0.2 photons per pulse.

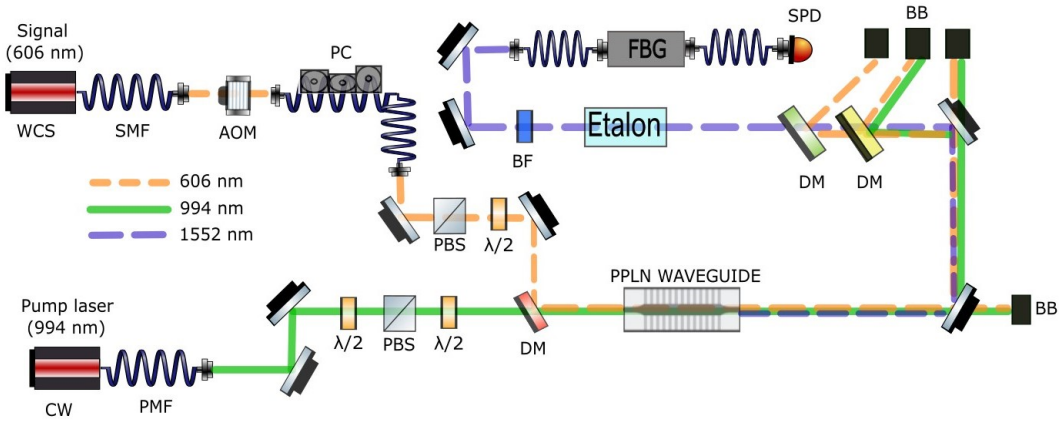

FIGURE 1: *Representation of the optical setup used for down-converting photons to telecom wavelengths. The dashed and continuous lines represent the pulse mode and continuous wave regime (CW) of light, respectively.*

5.1. Noise effects

We first describe the different noise processes that arise in a conversion experiment. The use of a strong pump field in QFC (down-conversion) can generate noise at the target wavelength, which is independent of the input signal power applied. The two primary noise processes are spontaneous parametric down-conversion (SPDC) and spurious spontaneous Raman scattering (SRS), [12] [13].

In SPDC a pump photon at 994 nm splits into a 1552 nm and a 2.77 μm photon. The SPDC noise extends for a large range of wavelengths within the transparency window of the waveguide (350 nm-4.5 μm) [12]. This particular type of noise is enhanced due to intrinsic arbitrary duty-cycle errors of the periodically poled structure of the waveguide [12]. Since the noise is broadband, it can be largely suppressed by using a narrow spectral filter.

The SRS noise, concretely Stokes SRS noise since $\lambda_T > \lambda_p$, is estimated to have a width of 48 THz in the PPLN waveguide. Therefore, SRS can only produce noise photons around the pump central frequency, becoming an irrelevant noise process for our scheme. Then, for the conversion from 606 nm to 1552 nm we have considered the SPDC as the dominant noise source.

5.2. Conversion efficiency

The conversion efficiency of our converter has been measured at the single photon level as function of the coupled pump power (see Figure (2)a), sending 200 ns (FWHM) every 100 μs at the input of the waveguide. We have a mean input value of 0.2 photons-per-pulse and a signal coupling of 45%. A maximum internal efficiency of 42% is achieved for an input pump power of 630 mW, 57% of which is coupled through the waveguide. This efficiency is calculated from the ratio of visible and telecom photons, at the input and

output of the waveguide, respectively, correcting for the signal coupling. The internal efficiency is then fitted by Eq. (1) (same approach as in Ref. [13]).

$$\eta_{QFC} = \eta_{max} \sin^2\left(\sqrt{\eta_{nor} P_c} L\right) \tag{1}$$

where η_{max} and η_{nor} are respectively the maximum and normalized efficiencies, L is the waveguide length and P_c is the coupled pump power.

The fit gives a maximum efficiency of 100% at 1.77 W of pump power and a normalized efficiency of $70\% W^{-1} cm^{-2}$. In addition, Figure (2)b shows an example of a histogram of the telecom counts measured over a pulse duration of 1.6 μs (FWHM). The considered detection window is 3.2 μs, which is twice the FWHM. The device efficiency accounts for all the possible optical losses before and after the waveguide i.e. from the first fiber coupled to the fiber connected to the detector. We finally obtain a device efficiency of 9.1% at the maximum pump power applied.

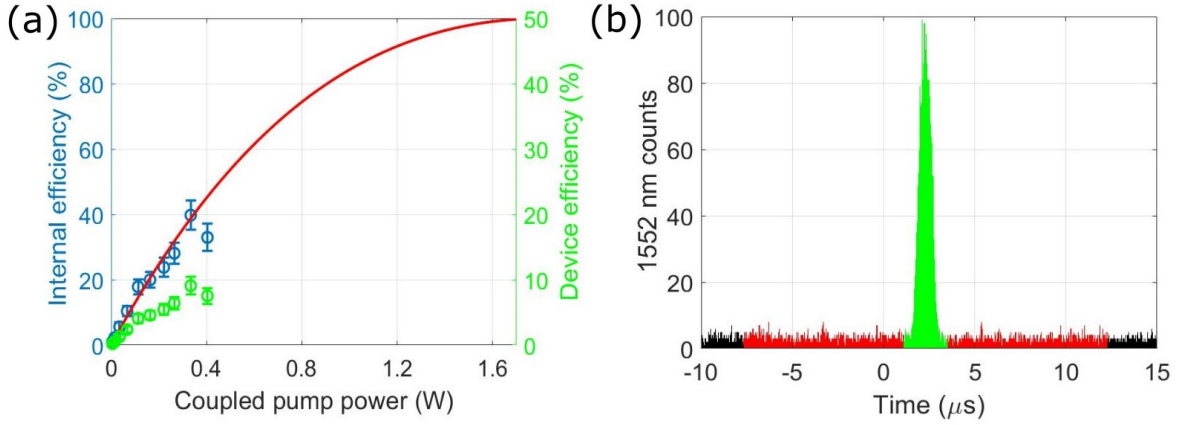

FIGURE 2: *(a) Internal (blue dots) and device (green dots) conversion efficiency as function of the coupled pump power. The red curve is a fit of the internal efficiency data using Eq. (1). (b) Histogram of a 1.6 μs (FWHM) Gaussian weak coherent pulse (green). In red, the window considered for the noise. The time bin is 10 ns.*

5.3. SNR and μ_1 measurements

In this thesis we define the SNR as the pure converted signal divided by the noise produced by the converter.

$$SNR = \frac{S}{N} = \frac{\mu_{in} \cdot \eta_{QFC} \cdot \eta_{loss}}{((R_{tel} \cdot \eta_{loss}) + R_{det}) \cdot \Delta t} \tag{2}$$

where μ_{in} is the mean input number of photons per pulse, η_{QFC} is the internal efficiency of our converter, η_{loss} refers to all the possible losses of the converted photons before and after the waveguide, R_{tel} is the telecom noise rate, R_{det} corresponds to the noise intrinsical to the detector (dark counts) and Δt is the pulse duration (FWHM). We

considered, as we show in Figure (2)b, the red window as the noise window to meausre it. A good model to estimate the noise is presented in Eq. (3) [7], which takes into consideration the up-conversion effect of part of the noise to 606 nm at high pump powers. The normalizing constant α_N, defined as the internal SPDC coefficient, corresponds to the linear slope for the first measured points of converted noise. We measured a value of 60 kHz/mW/cm normalized over 1 THz bandwidth.

$$R_{telecom} = \alpha_N P_c \left(L - \frac{\eta_{max}}{2} \left(L - \frac{\sin\left(2L\sqrt{\eta_{nor} P_c}\right)}{2\sqrt{\eta_{nor} P_c}} \right) \right) \tag{3}$$

Another measurement that can be used to assess the performance of the QFC device in terms of the SNR is the estimation of μ_1-parameter. This parameter is defined as the mean input number of photons per input pulse, μ_{in}, so that the SNR of the converted telecom photons is equivalent to 1, $\mu_1 = \frac{\mu_{in}}{SNR}$. It can be experimentally obtained by measuring the corresponding SNR, while varying the number of photons per pulse, and calculating the inverse of the resulting slope.

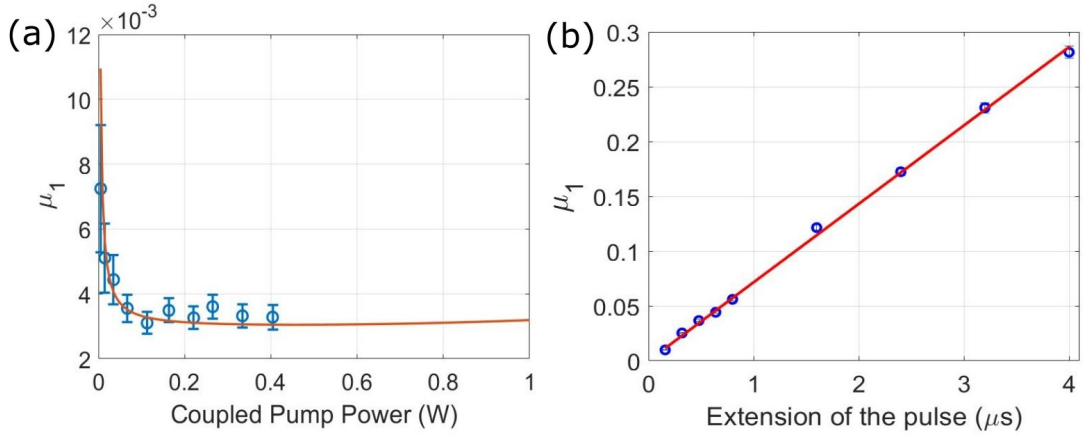

FIGURE 3: *Measurement of μ_1 of converted WCS as function of (a) the coupled pump power (b) the pulse duration (≈2·FWHM), together with the fit of the data. The 1552 nm converted photons are filtered with an etalon filter (210 MHz bandwidth) and a FBG (2.5 GHz bandwidth). Plot (a) is represented for a 0.023 mean number of photons per pulse and fitted based on Eq. (3). The measurement is made for a 200 ns detection window. In plot (b) the number of photons is kept constant for all durations and each measurement is made considering the full pulse. The error bars are hidden inside the dots.*

We characterize the QFC device by sending weak coherent states at 606 nm, compatible with praseodymium-based solid-state quantum memories. In Figures (3)a and (3)b we respectively show a measurement of μ_1 as function of the coupled pump power and the pulse duration. For Figure (3)a we have set 200 ns (FWHM) Gaussian pulses (same as in Ref. [7]). The μ_1-data is obtained by measuring the number of photons per pulse in front of the waveguide using a 606 nm detector (50% detection

efficiency) and dividing it by the SNR of the detected converted telecom photons. As we commented, part of the noise can be up-converted to 606 nm by the pump field via sum frequency generation (SFG), when the phase-matching condition is fulfilled. This explains the decrease of μ_1 in Figure (3)a. Nevertheless, once the conversion efficiency no longer compensates the converted noise we start to observe a saturating effect from μ_1, and even a degradation of its values. Interestingly, we achieve a value of $\mu_1 = (3.2 \pm 0.37) \cdot 10^{-3}$ at 404 mW coupled pump power, considering a 200 ns detection window (corresponding to the FWHM of the pulse). Considering the whole extension of the pulse (480ns) we measure a $\mu_1 = (9.92 \pm 0.26) \cdot 10^{-3}$. Regarding Figure (3)b, μ_1 presents a linear tendency with respect to the extension of the photon pulse, as we expected from Eq. (2) and the dependence of the SNR with μ_1. Extending the time window leads to considering more noise (SPDC). In addition, reaching a value of $\mu_1 < 0.3$ for 4 μs long pulse (110 kHz bandwidth) is promising for the use of QFC for connecting different narrowband quantum nodes such as trapped ions.

6. Calculation of converted cross-correlations via DLCZ-AFC protocol

As it was previously introduced, a Pr^{+3}:Y_2SiO_5 doped crystal is an excellent candidate for implementing QM protocols [14]. The $|g\rangle - |e\rangle$ (Pr^{+3} : $^3H_4$ - $^1D_2$) transition occurs at 606nm [11].The duration of the photons emitted from the current implementations of the DLCZ-AFC scheme is around 1 μs (FWHM). Working with longer photons would be promising as it would allow interfacing different types of quantum nodes.

To prove the preservation of photon quantum properties after conversion we can estimate the converted correlations between the Stokes and Anti-Stokes photons, in DLCZ-AFC protocol. Following the model of section (5) to compute the SNR (see Eq. (2)), the effect of noise on correlations can be deduced from (as in Ref. [15])

$$g^{(2)conv}_{DLCZ-AFC} = g^{(2)}_{DLCZ-AFC} \frac{SNR + 1}{SNR + g^{(2)}_{DLCZ-AFC}} \tag{4}$$

where $g^{(2)conv}_{DLCZ-AFC}$ ($g^{(2)}_{DLCZ-AFC}$) gives the converted (unconverted) second-order cross-correlations. We assume that the converted telecom photons are filtered with an etalon filter, the same used in section (5), and a Fabry-Pérot cavity (FPC) (98% transmission, 20 MHz linewidth, FSR=2 GHz). Therefore, one single frequency mode out of the several ones at the output of the etalon filter is selected. This FPC was designed during this thesis and will be built in the future. The use of this cavity should improve the SNR, and eventually μ_1, approximately by a factor of ten. The duration of the Anti-Stokes photon emitted is given by the extension of the read pulse sent, which we have set it to be 1 μs (FWHM). We assume that the window time is the same as the specified FWHM. Our signal is limited by DLCZ-AFC efficiency $\eta_{DLCZ-AFC}$. This efficiency, which is equivalent, in our case, to the input photon number in the QFC, is defined as the probability to retrieve an Anti-Stokes photon, heralded by the detection of a

Stokes photon. We have considered $\eta_{DLCZ-AFC}$ = 1.6% and a $g^{(2)}_{DLCZ-AFC}$=11.9, being the values obtained in the most recent experiment in our group [16] [17].

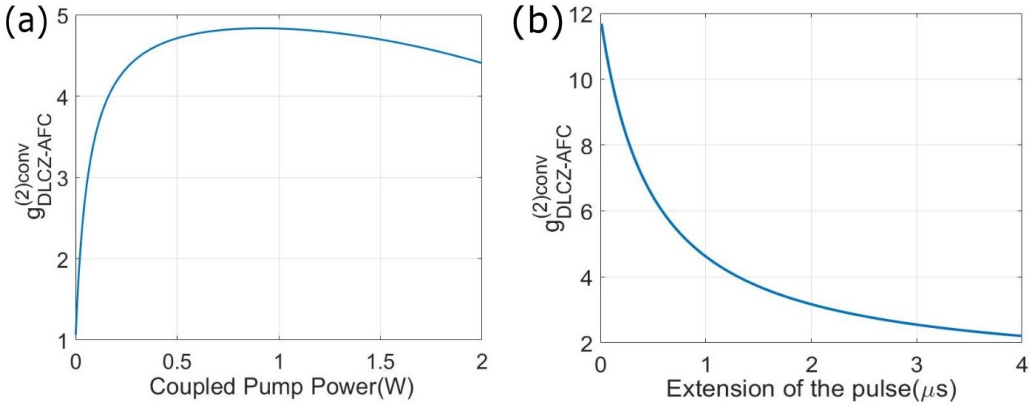

FIGURE 4: *QFC characterization. Expected behaviour of* $g^{(2)conv}_{DLCZ-AFC}$ *of down-converted photons produced by the DLCZ-AFC protocol as a function of the (a) pump power coupled into the waveguide and (b) pulse duration. All the parameters have been calculated following the model of Eq. (2) and (4), considering a DLCZ-AFC efficiency of 1.6% and a* $g^{(2)}_{DLCZ-AFC}$*=11.9. The 1552 nm converted photons are filtered with an etalon filter (210 MHz bandwidth) and a Fabry-Pérot cavity (20 MHz bandwidth), calculated over 1 μs integration window (FWHM). In plot (a) is set a 1 μs FWHM while in (b) we set a coupled pump power of 400 mW*

Figure (4)a shows the expected dependence of $g^{(2)conv}_{DLCZ-AFC}$ with the pump power. We can observe a linear tendency at low pump powers. However, when approaching 400 mW of coupled pump power the noise curve profile starts to saturate, which eventually affects the converted correlations profile in the same way. As we previously explained in section (5), part of the noise is back-converted to 606 nm via sum frequency generation (SFG). At higher coupled pump powers (>1.5W), $g^{(2)conv}_{DLCZ-AFC}$ values are degraded due to the decrease of conversion efficiency. In fact, we can observe a trade-off between the conversion efficiency and the converted cross-correlations (see Figures (2)a and (4)a). At 1.77 W of coupled pump power we can achieve a maximum conversion efficiency of 95%. However, at this power we do not reach the highest correlation value of 4.8. From Figures (4)a and (4)b we can observe that the telecom converted photons can exhibit non-classical converted cross-correlations (above the classical limit of 2) for the whole range of the coupled pump power (0W-2W) and the pulse duration (0μs-4μs) represented. As we have pointed out, noise effects predominate as the extension of the pulse is enlarged, decreasing the converted correlations.

7. Conclusions

In this thesis we have analyzed a frequency converter setup, aimed at down-converting light from 606 nm to the telecom wavelength 1552 nm. The relevance of this project lies

in its compatibility with the use of praseodymium doped-crystal quantum memories. In the characterization with WCS we measured a device conversion efficiency of 9.1% and a $\mu_1 = (3.2 \pm 0.37) \cdot 10^{-3}$ for a 200 ns detection window (FWHM) and the maximum coupled pump power applied ($\mu_1 = (9.92 \pm 0.26) \cdot 10^{-3}$, 480 ns detection window). We achieve meaningful μ_1-values for long pulse durations ($\mu_1 < 1$) with high applicability on single trapped ions, which linewidths are around 100 kHz. These values can be further enhanced by implementing a narrower-bandwidth filter such as a Fabry-Pérot cavity. Regarding the conversion of single photons via DLCZ-AFC protocol, we have theoretically shown non-classical correlations of the Stokes/Anti-Stokes photon pair after conversion and considering strong filtering. The increase of the DLCZ read-out efficiency and/or using a narrower filter would be necessary to further increase quantum correlations. For future work, we propose the implementation of an impedance-matching cavity [18] to improve the read-out efficiency.

Acknowledgements. I acknowledge my thesis advisor, Hugues de Riedmatten, Dr. Bernardo Casabone and Stefano Duranti for their guidance along the thesis.

8. References

[1] W. K. Wootters and W. H. Zurek, Nature **299**, 802–803 (1982).

[2] H.-J. Briegel, W. Dür, J. I. Cirac, and P. Zoller, Physical Review Letters **81**, 5932–5935 (1998).

[3] C. H. Bennett, G. Brassard, C. Crépeau, R. Jozsa, A. Peres, and W. K. Wootters, Phys. Rev. Lett. **70**, 1895–1899 (1993).

[4] L. M. Duan, M. D. Lukin, J. I. Cirac, and P. Zoller, Nature **414**, 413–418 (2001).

[5] Y.-L. Hua, Z.-Q. Zhou, C.-F. Li, and G.-C. Guo, Chinese Physics B, 020303 (2018).

[6] J. I. Cirac and P. Zoller, Physical Review Letters **74**, 4091–4094 (1995).

[7] N. Maring, D. Lago-Rivera, A. Lenhard, G. Heinze, and H. de Riedmatten, Optica **5**, 507 (2018).

[8] S. Tanzilli, H. de Riedmatten, W. Tittel, H. Zbinden, P. Baldi, M. De Micheli, D. Ostrowsky, and N. Gisin, The European Physical Journal D **18** (2001).

[9] P. Sekatski, N. Sangouard, N. Gisin, H. de Riedmatten, and M. Afzelius, Physical Review A **83** (2011).

[10] M. Afzelius, C. Simon, H. de Riedmatten, and N. Gisin, Physical Review A **79** (2009).

[11] Y. C. Sun, Spectroscopic Properties of Rare Earths in Optical Materials Springer Series in Materials Science, 379–429 (2005).

[12] J. S. Pelc, C. Langrock, Q. Zhang, and M. M. Fejer, Optics Letters **35**, 2804 (2010).

[13] S. Zaske, A. Lenhard, and C. Becher, Optics Express **19**, 12825 (2011).

[14] K. Kutluer, M. Mazzera, and H. de Riedmatten, Phys. Rev. Lett. **118**, 210502 (2017).

[15] B. Albrecht, P. Farrera, X. Fernandez-Gonzalvo, M. Cristiani, and H. de Riedmatten, Nature Communications **5** (2014).

[16] P. Farrera, G. Heinze, and H. de Riedmatten, Phys. Rev. Lett. **120**, 100501 (2018).

[17] K. Kutluer, E. Distante, B. Casabone, S. Duranti, M. Mazzera, and H. de Riedmatten, Phys. Rev. Lett. **123**, 030501 (2019).

[18] M. Afzelius and C. Simon, Physical Review A **82** (2010).